Yielding of overconsolidated sensitive clays due to unloading

Xiaoyang Cheng[1*], *and Minna* Karstunen[1]

[1] Department of Architecture and Civil Engineering, Chalmers University of Technology, Gothenburg, Sweden

Abstract. Natural slopes composed of overconsolidated sensitive clays are susceptible to large retrogressive flow slides that can occur rapidly once the soil structure is disturbed. Such disturbances may result from unloading processes. This study presents a series of anisotropically consolidated drained triaxial stress probing tests performed on intact samples of natural sensitive clay to investigate its yield response. Yield points are identified from multiple stress–strain plots to account for changes in anisotropy. Based on these results, the initial shape and size of the yield surface for the investigated material are determined. However, the portion of the yield surface on the dry side of the compression critical state requires further investigation, as sensitive clays exhibit a rapid increase in creep rate when approaching the Critical State Line (CSL). The experimental findings will be used to refine an existing constitutive model for sensitive clays, enhancing its capability to simulate the stress strain behaviour of sensitive clays during unloading.

1 Introduction

Over the decades, landslides have remained a persistent threat to infrastructure and human safety, particularly in regions characterised by sensitive clays, found in parts of Sweden, Norway, and Canada. Catastrophic events like the landslides in Gjerdrum (Norway) [1], Saint-Jude (Canada) [2], and Stenungsund (Sweden) [3] have highlighted the devastating consequences of slope failures in these areas.

As natural slopes made of sensitive clay have formed by erosion, they tend to be overconsolidated. Overconsolidated sensitive clays typically exhibit a brittle mechanical response characterized by pronounced strain softening, anisotropy, and rate-dependent behaviour [4]. Slopes composed of these materials are susceptible to large retrogressive flow slides that can occur rapidly once the soil structure is disturbed. Such disturbances may result from unloading processes caused by man-made cuts, natural erosion, or artesian groundwater conditions. In addition, natural overconsolidated clays tend to develop cracks and fissures due to unloading, which accelerates the reaction to environmental changes and further accelerates the instability of the slope. Therefore, understanding the response of natural sensitive clay during unloading is essential for reliable assessment of slope stability.

However, existing literature on unloading problems has primarily focused on underground excavations, where soils experience complex stress paths [5, 6], as illustrated in Fig. 1. Investigations of such unloading processes have relied largely on numerical analyses, which require robust constitutive models capable of capturing key features of soil behaviour, including anisotropy, rate-dependent mobilized shear strength, and small-strain stiffness [7-9]. In engineering practice, however, these parameters are typically derived from conventional triaxial compression tests, neglecting the influence of unloading stress paths. Systematic drained stress-probe tests on Chicago clay conducted by [10] demonstrated that stress–strain responses vary significantly with different stress paths.

As a first step, this study aims to investigate the yielding behaviour of natural sensitive clay through a series of drained triaxial stress-probe tests. The results are expected to facilitate the modification of existing clay constitutive models, which will subsequently be used to explore the mechanisms leading to slope failure induced by unloading.

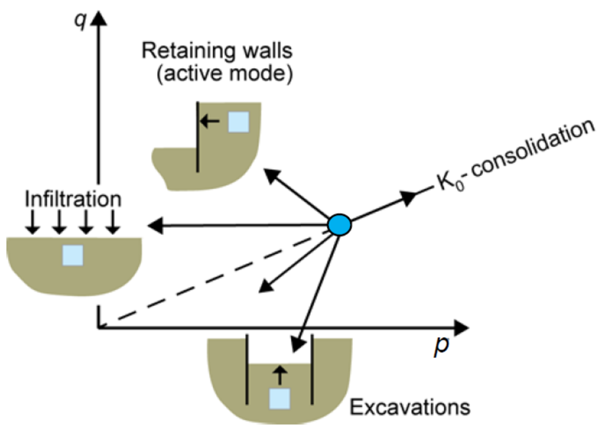

Fig. 1. Examples of unloading problems.

2 Experimental programme

A series of experimental tests have been performed on intact samples from Kärra test site in northern Gothenburg. Samples were retrieved from depths

* Corresponding author: chengxi@chalmers.se

between 9 and 10 m using the 50 mm Swedish STII piston sampler. The clay is characterized as lightly overconsolidated with an overconsolidation ratio (OCR) less than 2 [11]. The index properties of the clay are summarized in Table 1.

Table 1. Index properties of Kärra clay. ρ_b bulk density; LL: Liquid Limit; PL: Plastic Limit; PI: Plastic Index; w_N natural water content; S_t sensitivity (from fall cone).

Depth (m)	ρ_b (Mg/m^3)	LL (%)	PL (%)	PI (%)	w_N (%)	S_t
9	1.59	75	28	47	72	8
10	1.59	73	29	44	72	10

All triaxial tests were conducted on cylindrical specimens with a diameter of 50 mm and a height of 100 mm using GDS Bishop–Wesley triaxial cells at a constant temperature of 7 °C. Paraffin oil was used as the cell fluid to eliminate the need for membrane correction. Back pressure was applied at the top of the specimen, while pore water pressure was measured at the base. A suction cap was employed to enable extension loading and to ensure proper alignment of the applied load between the load cell and the top platen. In all tests, filter paper side drains were used to accelerate consolidation.

After docking of the sample, each sample was saturated by simultaneously increasing the cell pressure and back pressure to a final back pressure of 150 kPa. A Skempton *B* value of at least 0.95 was adopted as the criterion for full saturation. Following saturation, the specimens were consolidated to the estimated in situ effective stress state using a coefficient of earth pressure at rest of $K_0 = 0.6$, corresponding to the stress path from point 0 to point A in p'–q space (mean effective stress vs. deviatoric stress) in Fig. 2. From point A, the specimens were subjected to a series of drained stress probes under stress-controlled conditions. A low stress rate of 0.05 kPa/h was adopted to minimize the generation of excess pore water pressure during probing.

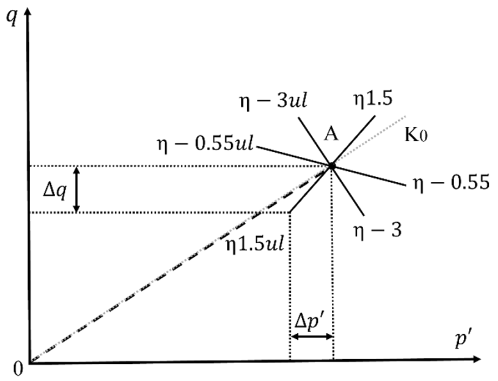

Fig. 2. Schematic of testing program.

Details of the triaxial testing program are summarized in Table 2, including the sample depth, initial void ratio e_0, in situ vertical and (estimated) horizontal stresses and stress ratio η. In the notation describing each test in Fig. 2 and Table 2, the number attached to 'η' represents the value of stress ratio, and the suffix 'ul' denotes the unloading stress paths. Herein, loading refers to the paths where mean effective stress *p*' increases, while unloading paths represent the paths where *p*' decreases. The testing programme comprises three drained triaxial tests conducted along unloading stress paths, with stress ratios η (= $\Delta q/\Delta p'$) of 1.5, −0.55, and −3, respectively, to investigate the unloading response of natural overconsolidated clay. For comparison and characterization of loading behaviour of the testing site, three additional drained triaxial tests with the same stress ratios but in the opposite direction were performed.

Table 2. Triaxial testing program.

Test name	Depth (m)	e_0	Initial stress (kPa)		Stress ratio
			σ_a'	σ_r'	
η1.5	10	1.71	58	34.8	1.5
η1.5ul	9	1.81	52.2	31.3	1.5
η-0.55	9	1.85	52.2	31.3	-0.55
η-0.55ul	9	1.77	52.2	31.3	-0.55
η-3	10	1.72	58	34.8	-3
η-3ul	10	1.76	58	34.8	-3

The mean effective stress *p'* and the deviatoric stress *q* can be calculated as follows:

$$p' = \frac{\sigma'_a + 2\sigma'_r}{3} \quad (1)$$

$$q = \sigma'_a - \sigma'_r \quad (2)$$

where σ_a' and σ_r' stand for the axial stress and confining pressure, respectively. The corresponding volumetric strain ε_v and deviatoric strain ε_q can be defined as:

$$\varepsilon_v = \varepsilon_a + 2\varepsilon_r \quad (3)$$

$$\varepsilon_q = 2/3(\varepsilon_a - \varepsilon_r) \quad (4)$$

where ε_a and ε_r are the axial and radial strains, respectively. The positive sign means compression, while the negative sign means extension.

3 Results

3.1 Stress paths

Fig. 3 presents an overview of the actual stress paths for the six triaxial tests in *p'*-*q* stress space. Overall, the stress paths closely follow the target stress ratios. The two stress path η1.5 and η-3 tend to approach the critical state lines (CSLs) with a stress ratio of *Mc* = 1.5 and *Me* = 1.2 for compression and extension, respectively. This result is consistent with results from conventional undrained triaxial compression and extension tests conducted on the same clay by [11].

It should be noted that, because the tests were stress-controlled, the strain rate varied throughout the loading process. As the stress state approached the CSL, this variation led to the generation of excess pore water pressure, as shown in Fig. 4. Even for the stress path designed to be parallel to the CSL in compression (test η1.5), specimen failure occurred suddenly due to the development of significant excess pore water pressure associated with large shear strains.

In contrast, test η−0.55ul crossed the CSL without failure. The test was terminated manually to avoid the confining pressure being reduced below the applied back pressure.

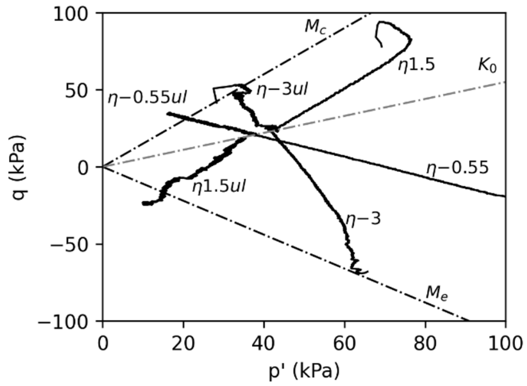

Fig. 3. Actual stress paths.

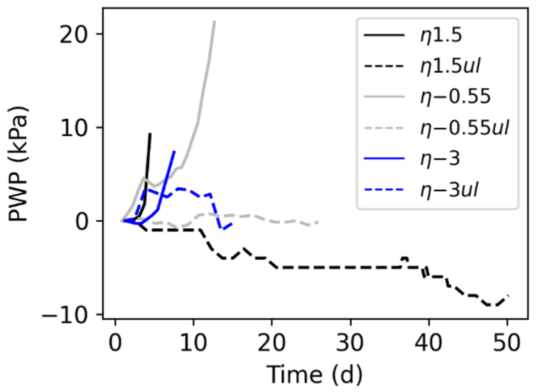

Fig. 4. Evolution of excess pore water pressure (PWP).

3.2 Yield response

3.2.1 Determination of yield points

The yield points for each stress path in this study were determined using the bilinear elasto-plastic method, in which the yield point is typically identified as the intersection of rectilinear extrapolations of the pre-yield and post-yield segments in the p'–ε_v plane. However, considering the changes in anisotropy and bonding in sensitive clays with some stress paths, [12] recommended the use of additional plots, such as q–ε_v, to verify the identified yield points. Figs. 5–10 present the yield points (blue dots) identified from both the p'–ε_v and q–ε_v plots for all tests, and the results are summarized in Table 3.

For test η = 1.5 (Fig. 5), the rapid build-up of pore water pressure causes a sharp reduction in p' in the post-yield stage, as shown in Fig. 5a. Consequently, the available data for fitting the post-yield segment in the p'–ε_v plot is limited, which may reduce the accuracy of the bilinear approximation. In the q–ε_v plot in Fig. 5b, both the pre-yield and post-yield portions of the curve can be more accurately approximated by two straight lines. The p'–ε_v plot suggests a yield point of p'_c = 72.5 kPa, whereas the q–ε_v plot indicates p'_c = 74.7 kPa, as shown in Table 3.

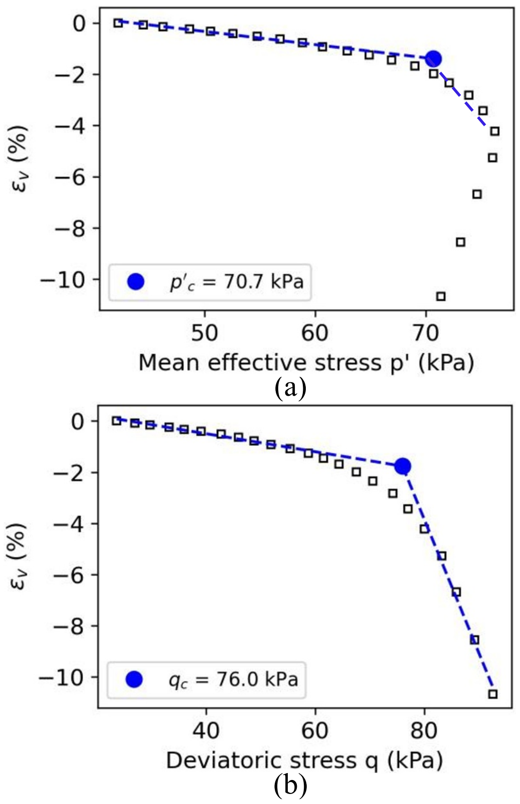

Fig. 5. Yield points determined from curves (a) ε_v–p' and (b) ε_v–q for test η1.5.

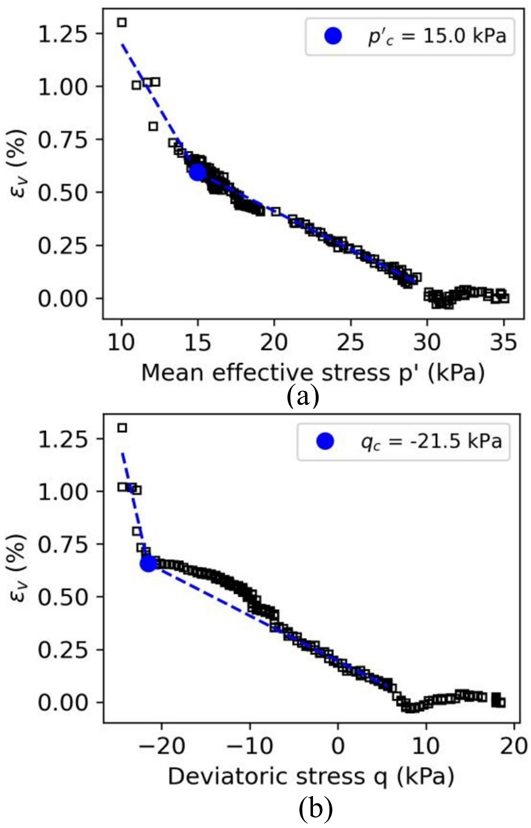

Fig. 6. Yield points determined from curves (a) ε_v–p' and (b) ε_v–q for test η1.5ul.

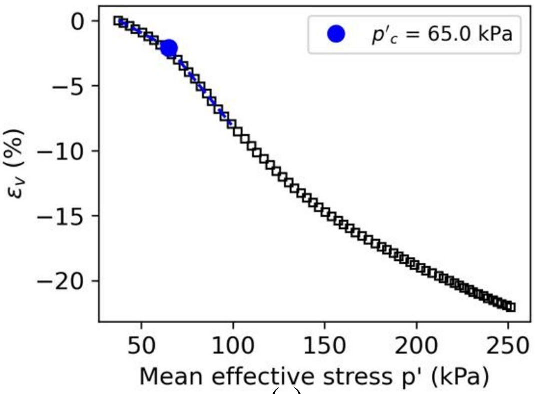

(a)

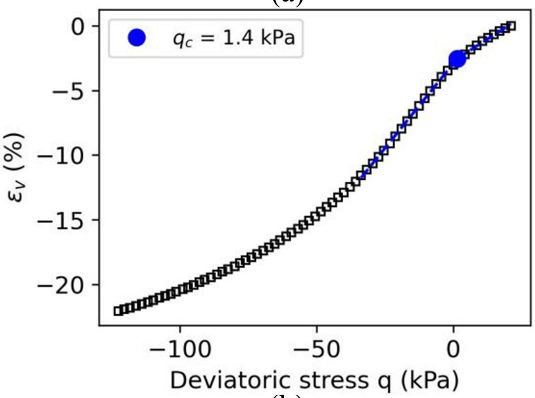

(b)

Fig. 7. Yield points determined from curves (a) ε_v−p' and (b) ε_v−q for test η-0.55.

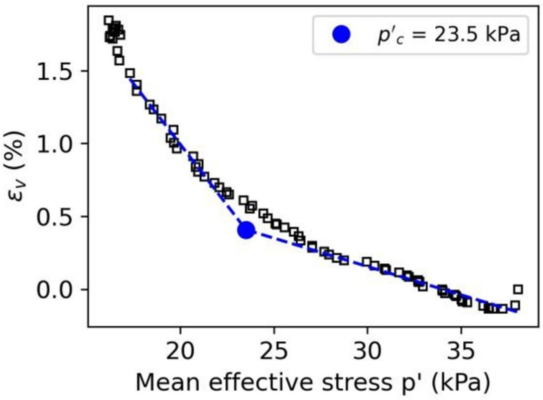

(a)

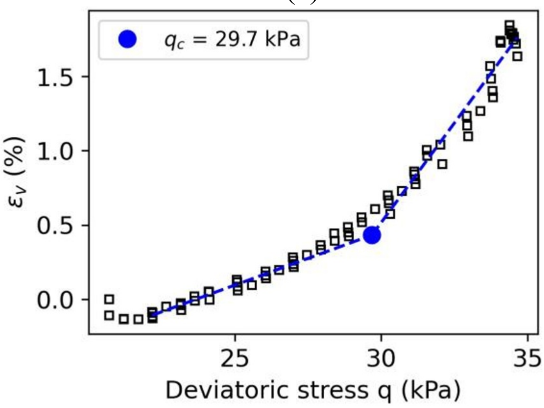

(b)

Fig. 8. Yield points determined from curves (a) ε_v−p' and (b) ε_v−q for test η-0.55ul.

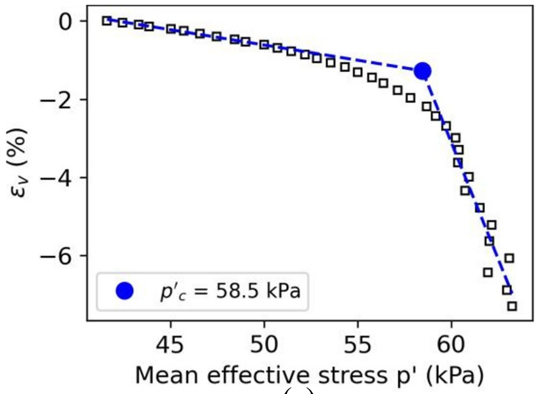

(a)

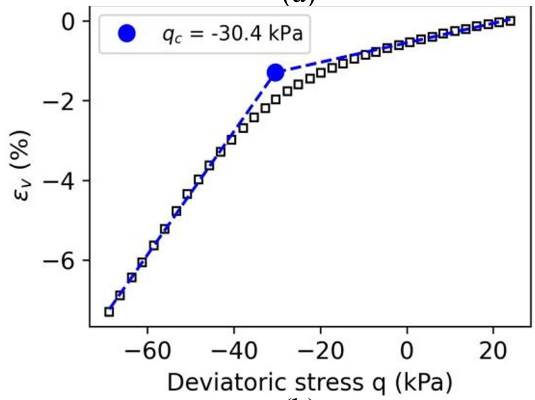

(b)

Fig. 9. Yield points determined from curves (a) ε_v−p' and (b) ε_v−q for test η-3.

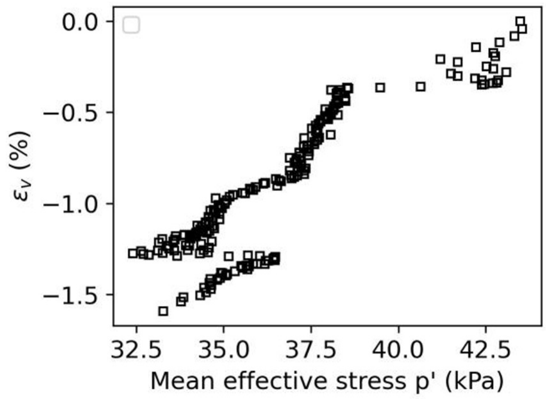

(a)

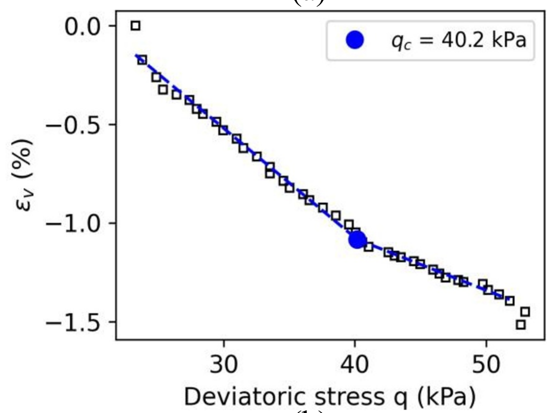

(b)

Fig. 10. Yield points determined from curves (a) ε_v−p' and (b) ε_v−q for test η-3ul.

Table 3. Yield points obtained from different stress strain responses.

Test name	p' - ε_v		q - ε_v	
	p_c'	q_c	p_c'	q_c
η1.5	72.5	67.6	74.7	76
η1.5ul	15	-17.2	14.4	-21.5
η-0.55	65	3.8	70.4	1.4
η-0.55ul	23.5	29.3	23.0	29.7
η-3	58.5	-31.6	57.8	-30.4
η-3ul	-	-	34.5	40.2

For unloading test η1.5ul (Fig. 6), two apparent turning points are observed – at approximately p' = 30 kPa and p' = 15 kPa in Fig. 5a, corresponding to q = 10 kPa and q = -20 kPa in Fig. 5b. During the initial stage of unloading, from approximately p' = 35 to 30 kPa (corresponding to q = 20 to 10 kPa), both volumetric and deviatoric strains exhibit negligible changes. This weak response is likely associated with the relocation of the suction head. Therefore, the second turning point is interpreted as the yield point, and the corresponding yield stresses p_c' identified from the two plots are in good agreement, as indicated in Table 3.

The yield points are evident in both p'–ε_v and q–ε_v plots for test η-0.55, η-0.55ul and η-3 as shown in Figs.7-9. It is difficult to interpret the p'–ε_v for test η-3ul in Fig. 10a due to the significant noise. However, the yield point can be readily identified from q–ε_v plot in Fig. 10b.

In summary, the yield points obtained from p'–ε_v and q–ε_v plots generally display almost identical values. Using both representations allows the identified yield points to be cross-checked and helps to compensate for stress paths where the yield point is not clearly defined in either the p'–ε_v or q–ε_v curve alone.

3.2.2 Yield surface

An average value of the yield points in Table 3 was therefore adopted as the final yield point for each test. The yield surface was obtained by mapping these points in the p'-q space as shown in Fig. 11. As the specimens were retrieved from different depths, the yield points were normalized by the corresponding in situ mean effective stresses p'_0, equal to 38.3 kPa and 42.5 kPa for depths of 9 m and 10 m, respectively. The CSLs determined from Fig. 3 are also included for reference.

The yield surface of Creep-SCLAY1S model [13, 14] described by Equation (5) is used to fit the experimental data:

$$f_{yield} = (q-\alpha p')^2 - (M^2-\alpha^2)(p'_m - p')p' \qquad (5)$$

where α is the inclination of the yield surface. p′m represents the preconsolidation pressure. The value of stress ratio at critical state M is taken from Fig. 3. The initial inclination of the yield surface α0 takes a value of 0.58, which can be derived from:

$$\alpha_0 = \frac{\eta_{K_0^{NC}}^2 + \eta_{K_0^{NC}} - M_c^2}{3} \qquad (6)$$

with

$$\eta_{K_0^{NC}} = \frac{3(1-K_0^{NC})}{1+2K_0^{NC}} \qquad (7)$$

$$K_0^{NC} = 1 - sin\varphi' \qquad (8)$$

where K_0^{NC} is the lateral earth pressure at rest for normally consolidated state. $\eta_{K_0^{NC}}$ is the value of the stress ratio in K_0^{NC} loading. Details can be found in [14]. Overall, the agreement between the predicted yield locus and the experimental data for the loading test is satisfying on the “wet” side of critical state.

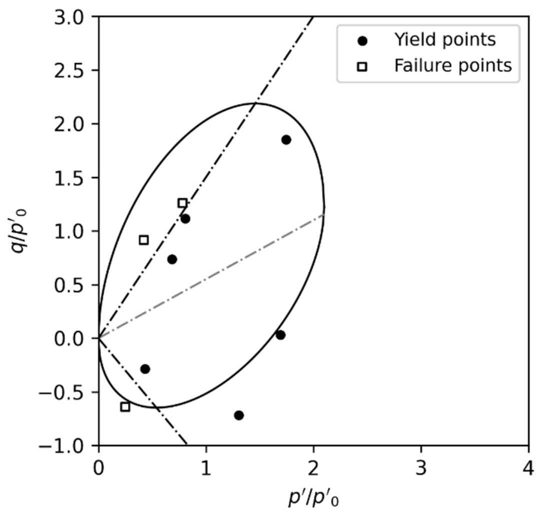

Fig. 11. Fitted yield surface in p'-q stress space with α_0 = 0.58.

The yield points for the unloading stress paths, however, lie close to the CSL. The failure points located at dry side of CSLs for unloading tests are therefore included to fit the model. As test η−0.55ul didn’t reach failure, its final recorded point is presented instead. It is expected that the failure point for test η−0.55ul would theoretically be located closer to the yield curve if the stress path were continued. In contrast, test η−3ul failed at an earlier stage due to the rapid increase in creep rate as the stress path approached the CSL in compression [15]. Given these experimental limitations, it is reasonable to assume that the yield locus fits better the failure points than the yield points for the unloading stress paths that reach dry side. By fitting the proposed equation to the experimental data, an isotropic OCR* (=p'_m/p'_{eq}) value of 2.1 was obtained, which is comparable to that reported in [11]. Here, p'_{eq} denotes the equivalent isotropic mean effective stress.

4 Conclusions

This paper presents the results of an experimental programme aimed at characterizing the yielding response of intact sensitive clay due to unloading. The testing programme comprised six drained directional stress-probe tests initiated from in situ K_0 stress conditions. Based on the experimental results, the following conclusions can be drawn:

- The yield points identified from both the p'–ε_v and q–ε_v curves are generally in good agreement and can therefore be used to cross-check and complement each other.
- The Creep-SCLAY1S model is generally capable of reproducing the yield behaviour of sensitive clay under loading conditions.
- The yield points identified from unloading stress paths are located close to the critical state lines (CSLs). Experimentally loading sensitive clay to the dry side of the compression critical state at high stress ratios is difficult due to the rapid increase in creep rate as the stress path approaches the CSL. Consequently, the experiments tend to provide more reliable predictions of failure points than of yield points.

This preliminary study establishes a foundation for further investigation into the unloading response of overconsolidated sensitive clays. The expanded experimental database will be used to refine existing constitutive models to better capture unloading behaviour and will subsequently be applied to the simulation of cut slopes and underground excavations.

The work is funded by Formas (Research Council for sustainable Development) (Grant 2021-02400), Swedish Research Council (VR 2024-04672) and Swedish Transport Administration (Grant 2022/69758) via BIG (Branch-samverkan in grunden). The work is done as part of Digital Twin Cities Centre that is supported by Sweden's Innovation Agency VINNOVA (Grant 2024- 03904).

References

1. G. Devoli, I. Skrede, E. Haugen, T. Wiig, Scarp monitoring, early warning and documentation of successive landslides occurred after the quick clay slide in Ask, Gjerdrum (Norway). In IOP Conference Series: Earth and Environmental Science. Vol. **1523**, No. 1, p. 012040 (2025).
2. A. Locat, P. Locat, D. Demers, S. Leroueil, D. Robitaille, G. Lefebvre, The Saint-Jude landslide of 10 May 2010, Quebec, Canada: Investigation and characterization of the landslide and its failure mechanism. Can. Geotech. J. **54**(10), 1357-1374 (2017). https://doi.org/10.1139/cgj-2017-0085@cgj-ec.2017.01.issue-6
3. M. Georgsson, A. Lindqvist, En rasande detaljplaneprocess-Jordskredet i Stenungsund: En undersökande studie om jordskredet i Stenungsund, 2024.
4. K.-Y. Lo, J.-P. Morin, Strength anisotropy and time effects of two sensitive clays. Can. Geotech. J. **9**(3), 261-277 (1972). https://doi.org/10.1139/t72-030
5. W. Huang, J. Li, Y. Lu, D. Li, Y. Mou, X. Wu, Z. Li, Mechanical properties of soft soil considering the influence of unloading stress paths. Adv. Civ. Eng. **2021**(1), 8813882 (2021). https://doi.org/10.1155/2021/8813882
6. R. Ignat, S. Baker, M. Holmén, S. Larsson, Triaxial extension and tension tests on lime-cement-improved clay. Soils and Foundations. 59(5), 1399-1416 (2019). https://doi.org/10.1016/j.sandf.2019.06.004
7. S.-J. Wheeler, A. Näätänen, M. Karstunen, M. Lojander, An anisotropic elastoplastic model for soft clays. Can. Geotech. J. **40**(2), 403-418 (2003). https://doi.org/10.1139/t02-119
8. F. Scharinger, H.-F. Schweiger, G.-N. Pande, On a multilaminate model for soil incorporating small strain stiffness. Int. J. Numer. Anal. Meth. Geomech. **33**(2), 215-243 (2009). https://doi.org/10.1002/nag.710
9. T. Wood, On the small strain stiffness of some Scandinavian clays and impact on deep excavation. Doctoral dissertation. Chalmers University of Technology, Sweden, 2016.
10. T. Kim, Incrementally nonlinear responses of soft Chicago glacial clays, Doctoral dissertation, Northwestern University, 2011.
11. H. Tahershamsi, R.-A. Naghadeh, B.-Z. Coelho, J. Dijkstra, Low amplitude strain accumulation model for natural soft clays below railways. Transp. Geotech. **42**, 101011(2023). https://doi.org/10.1016/j.trgeo.2023.101011
12. M. Koskinen, M. Karstunen, M. Lojander, Yielding of" ideal" and natural anisotropic clays. In International Workshop on Geotechnics of Soft Soils, Noordwijkerhout, The Netherlands, 17-19 September 2003 (pp. 197-204).
13. N. Sivasithamparam, M. Karstunen, P. Bonnier, Modelling creep behaviour of anisotropic soft soils. Computers &. Geotechnics **69**, 46-57 (2015). https://doi.org/10.1016/j.compgeo.2015.04.015
14. J.-P. Gras, N. Sivasithamparam, M. Karstunen, et al., Permissible range of model parameters for natural fine-grained materials. Acta Geotechnica **13**, 387–398 (2018). https://doi.org/10.1007/s11440-017-0553-1
15. S. Leroueil, R.-J. Chandler, Natural slopes and cuts: movement and failure mechanisms. Géotechnique, **51**(3), pp.197-243 (2001). https://doi.org/10.1680/geot.2001.51.3.197